

An improved method to access initial states in relativistic heavy-ion collisions

Somadutta Bhatta¹ and Vipul Bairathi^{2a}

¹ Department of Chemistry, Stony Brook University, Stony Brook, NY 11794, USA

² Instituto de Alta Investigación, Universidad de Tarapacá, Casilla 7D Arica 1000000, Chile

Received: date / Revised version: date

Abstract. Observables in heavy-ion collisions are generally categorized into centralities, which reflect an average over events within a range of impact parameter including a wide variety of initial state configurations. A multiple binning method using spectator neutrons within each centrality has been previously shown to provide access to events with rare initial state conditions. This work suggests an improvement in quantifying the difference between standard centrality and spectator neutron binning towards accessing the initial state properties. A selection of events with higher initial state density at fixed participating nucleon number was observed to result in larger final state particle production and smaller elliptic flow. The relative difference between observables in centrality and spectator binning shows reduced sensitivity for the observables dominated by impact parameter fluctuations in initial state such as triangular flow. This property makes the spectator binning method a good candidate to separate geometric contributions from random fluctuations in initial state towards final state observables.

PACS. PACS-key describing text of that key – PACS-key describing text of that key

Send offprint requests to:

^a Present address: vipul.bairathi@gmail.com

1 Introduction

In relativistic heavy-ion collisions, a large amount of energy deposited in the collision region deconfines the hadronic matter into strongly-interacting medium called Quark-Gluon Plasma (QGP) [1,2]. Subsequent cooling and expansion of the QGP leads to the production of particles, which carry important information about the initial state of the collision. Initial states of heavy-ion collisions are very important and poses one of the biggest challenges in understanding the properties and dynamics of the QGP medium produced in relativistic heavy-ion collisions. State-of-art Bayesian analyses are generally used to constrain the transport properties of the QGP. But, a large uncertainty in these analyses arises from the specific assumptions on the initial state prior to hydrodynamic expansion [3,4,5]. For example, depending on the choice of initial conditions made in modeling of heavy-ion collisions, the extracted values of shear viscosity to entropy density ratio at the RHIC can vary by a factor of 2 [6,7,8,9,10,11].

One of the primary variables controlling the amount of energy deposited in the collision region is impact parameter (b) i.e the transverse distance between the center of two colliding nuclei. Collision events are categorized into “centralities” which directly correlates to b . In model calculations, the total number of participating nucleons is used for centrality definition. Whereas, number of charged particles (N_{ch}) in a given pseudorapidity (η) region is used in experiments to define event centrality. In a simple Monte Carlo Glauber model simulation of heavy-ion collisions, initial state observables (e.g. transverse overlap area (S), eccentricity of overlap region (ε_n), number of participating nucleons (N_{part}) and number of binary collisions (N_{coll})) show monotonicity as a function of event centrality [12,13]. The pressure gradient in initial state converts the spatial eccentricity to final state momentum anisotropy. This final state asymmetry is quantified by a Fourier expansion of azimuthal distribution of particles. The second and third coefficients in the Fourier expansion are called elliptic (v_2) and triangular flow (v_3), respectively [14,15]. Existing transport models and hydrodynamic simulations describe the evolution of final state observables as a function of centrality [16,17,18,19,20]. But, the current model predictions are dependent on the choice of initial state in heavy-ion collisions.

Estimates of initial state parameters and measurements of final state observables as a function of centrality only reflects the mean values over events within a centrality range. However, such averaging procedure limits detailed access to the initial state configurations contributing to the mean. The spectator nucleons (N_{spec} , defined as N_{part} subtracted from total number of nucleons), is an event property that also has a strong correlation to the impact parameter and can be used to categorize events on a similar footing as N_{part} or N_{ch} . Simply put, N_{spec} in an event is anti-correlated to the N_{part} . Ref. [21] showed that N_{spec} carries the initial state information, which can be used to select specific collision configurations such as body-tip in deformed Uranium nuclei.

Despite the strong correlation between N_{spec} and N_{part} , the N_{ch} has been shown to have a reduced correlation with the N_{spec} stemming from interactions and scatterings in the overlap region [22]. The exact magnitude of the correlation between N_{spec} and N_{ch} might vary depending on the η in which N_{ch} is defined. The reduction in correlation between N_{ch} and N_{spec} forms a basis to use N_{spec} as an approximately independent and new classifier of events. The advantage of such binning procedure in accessing the wide variety of initial state for events within any given centrality has already been studied and reported in Refs [21,23]. In heavy-ion experiments, it is only possible to get information on the number of spectator neutrons. Therefore, we define n_{spec} as the sum of neutron spectators going towards left and right direction along the collision axis. In relativistic heavy ion collider (RHIC) at BNL, two Zero-Degree-Calorimeters (ZDC) placed at $|\eta| > 6.0$ capture the spectator neutrons coming from the interaction region along the beam pipe [24, 25]. Ref [24] reported the single neutron peak resolution of $\sigma_E/E \sim 40\%$ in peripheral collisions of Au+Au nuclei with current STAR ZDC, owing to clustering of relatively larger number of neutrons. Therefore, we limit our measurements to 0–60% centrality range in this study.

Before using this novel method to understand initial state properties of heavy-ion collisions, it is important to develop simple method that could differentiate between the extent of information on initial state obtained from centrality classification and n_{spec} classification of events. In addition, model simulations provide a better understanding of the behavior of observables when plotted as a function of aforementioned event classifiers. Therefore, in this work, we used a transport model to compare observables between: (i) a centrality event classifier based on N_{ch} cuts (“centrality binning”) and (ii) a multiple binning procedure in which events within a given centrality are further classified into several sub-groups using n_{spec} as an event classifier (“L+R binning”).

This paper is structured as follows. Section 2 describes the justification for the new methodology used and suggested improvements in event classification. We present our results and discuss them in Section 3. Lastly, in Section 4 we summarize our findings and provide outlook.

2 Methodology

A Multi Phase Transport (AMPT) [26] model in the string melting version is used to simulate collision events for this study. The AMPT model uses the same initial conditions as HIJING [27]. Zhang’s parton cascade [28] follows to take into account partonic interactions which finally recombine with their parent strings that fragment into hadrons within the Lund String Fragmentation model [29]. There is a final stage hadronic afterburner before the hadrons freezeout. The AMPT model has been shown to reproduce experimentally measured observables such as collective flow and

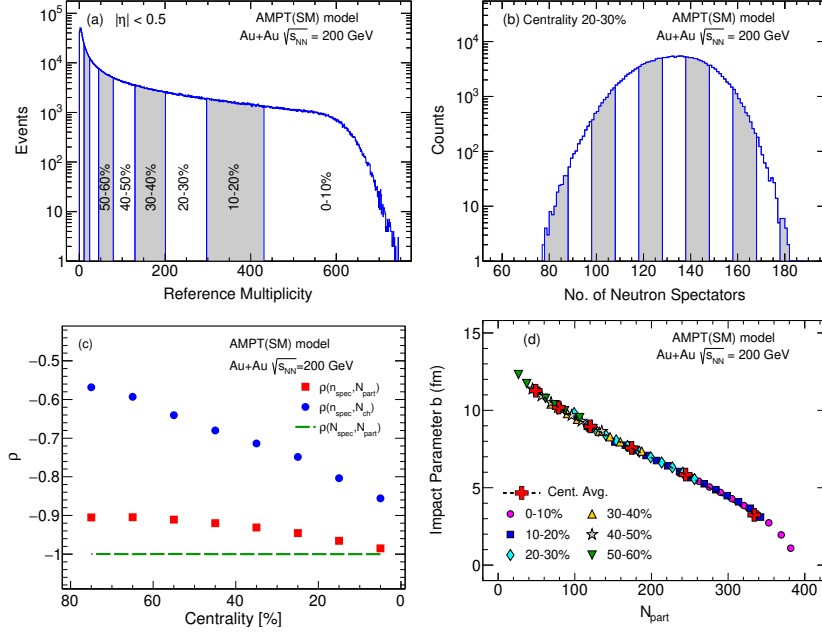


Fig. 1. (Color online) (a) The multiplicity in $|\eta| < 0.5$ (N_{ch}) for minimum bias Au+Au collisions at $\sqrt{s_{NN}} = 200$ GeV. In alternate white and grey bands, different centrality bins from 0-10% to 70-80% are shown. (b) The total spectator neutron number (n_{spec}) distribution for 20-30% centrality. The different L+R bins are shown in alternate white and grey bands. (c) Pearson correlator between $N_{spec}-N_{part}$ (solid line), $n_{spec}-N_{part}$ (solid box) and $n_{spec}-N_{ch}$ (solid circle) as a function of centrality for Au+Au collisions at $\sqrt{s_{NN}} = 200$ GeV (d) The impact parameter (b) vs N_{part} for different centrality and L+R bins.

$dN_{ch}/d\eta$ to a good approximation [19,20]. In this work, ~ 2 million Au+Au collision events at $\sqrt{s_{NN}} = 200$ GeV are simulated.

The method of multiple binning used in this study follows Ref. [23]. We provide a brief outline of this procedure here. The centrality of an event is defined based on N_{ch} which is calculated within $|\eta| < 0.5$. Based on percentile of N_{ch} distribution, events are classified into 8 centrality bins each of 10 percentile as shown in Fig. 1(a) for Au+Au collisions at $\sqrt{s_{NN}} = 200$ GeV. The n_{spec} distribution in each of the 8 centralities is further divided into regular intervals of n_{spec} as shown in Fig. 1(b) for 20–30% centrality. The n_{spec} distribution displays a prominent peak around 125-140 and falls off rapidly on either side. The averaging over events within a centrality range in centrality binning reflects properties of the events around the peak of total spectator neutrons distribution. We can investigate properties of the rare events with fewer or higher values of n_{spec} compared to the central value with the introduction of the L+R binning.

Pearson correlators are widely used to quantify the correlations between any two observables in experimental heavy-ion collisions [22,30,31]. To emphasize the reduction in correlations between N_{ch} and n_{spec} in comparison to N_{part}

and n_{spec} , two Pearson correlators are defined on an event by event basis, $\rho(n_{\text{spec}}, N_{\text{part}})$ and $\rho(n_{\text{spec}}, N_{\text{ch}})$. Fig. 1(c) shows comparison between $\rho(N_{\text{spec}}, N_{\text{part}})$, $\rho(n_{\text{spec}}, N_{\text{part}})$ and $\rho(n_{\text{spec}}, N_{\text{ch}})$ as a function of centrality. The N_{spec} is mathematically anti-correlated to N_{part} which results in a $\rho(N_{\text{spec}}, N_{\text{part}})$ of -1, irrespective of centrality. But, owing to the fact that we use number of spectator neutrons for the correlation measure (not total number of spectators) and due to event-by-event fluctuations, the magnitude of $\rho(n_{\text{spec}}, N_{\text{part}})$ shows small deviations from the expected value of -1. In addition, as we go from central to peripheral centralities, the absolute magnitude of $\rho(n_{\text{spec}}, N_{\text{part}})$ is observed to decrease by about 10%, which might be due to increased fluctuation contributions to the spectator numbers with decreasing overlap area. In contrast, the absolute magnitude of $\rho(n_{\text{spec}}, N_{\text{ch}})$ is observed to decrease by about 45% going from central to peripheral events. Because N_{ch} and n_{spec} are very weakly correlated, classifying events with n_{spec} on top of N_{ch} is expected to give us increasingly more details on event properties in relatively peripheral events. In real experiments, the exact magnitude of correlation between N_{spec} and $dN_{\text{ch}}/d\eta$ might be different than those observed here, but the overall behavior is expected to remain the same. It might also be of interest to compare $\rho(n_{\text{spec}}, N_{\text{ch}})$ as a function of centrality between systems of different sizes to further understand its origin.

For centrality binning, observables are averaged over centrality intervals of 10% each. For L+R binning, observables are calculated by taking an average over equally spaced L+R bins within any given centrality. Fig. 1(d) shows the variation of b with N_{part} in which centrality and L+R bins are observed to follow the same trend. This implies that the L+R bins in any given centrality can be used to select events with similar impact parameter and N_{part} as the usual centrality binning. Thus, introduction of n_{spec} as an additional event classifier does not intrinsically select on events with different centrality and thus does not bias our event selection. Therefore, any deviation from the centrality averaged trend, if observed in L+R binning allows access to novel initial state configurations in heavy-ion collisions.

3 Results

This work focuses on the additional insights obtained from L+R binning on top of centrality binning. The observables considered are N_{part} , N_{coll} , N_{ch} , S , ε_n and v_n for $n = 2, 3$. The transverse overlap area is calculated as $S = \pi \sqrt{\sigma_x^2 \sigma_y^2}$, where σ_x and σ_y are defined as $\sqrt{\langle x^2 \rangle - \langle x \rangle^2}$ and $\sqrt{\langle y^2 \rangle - \langle y \rangle^2}$, respectively and (x, y) denote the position of participating nucleons in the transverse plane. Eccentricities $\varepsilon_n = -\langle r^n e^{-in\phi} \rangle / \langle r^n \rangle$ are calculated from the positions (r, ϕ) of participating nucleons in the transverse plane. The coordinate system is shifted to center of mass of participating nucleons. The calculation of the initial state observables closely follows Ref. [32]. For estimation of final state flow coefficients, Event-plane method is used [14]. In this method, the reaction plane angle is estimated by event plane angle for each harmonic and the azimuthal anisotropy of particles are calculated about this plane [14].

Figure 2(a) shows S as a function of N_{part} . For centrality averaged values, the initial overlap area increases from peripheral to central collisions due to decrease in impact parameter. The correlation between S and N_{part} is different between L+R binning and centrality binning. In L+R binning S rises faster than centrality averaged trend. The difference between trends shown by L+R and centrality binning is dependent on event centrality. Using L+R bins, it is possible to access events with a wider range of S and N_{part} compared to centrality averaged values in any given centrality. In addition, at a given N_{part} , we could choose events with different S using L+R binning, which could help in studying the impact of initial participating nucleon density on final state observables. At a fixed N_{part} , the area in L+R binning for more central events is observed to be smaller than that of a comparatively peripheral centrality. Thus, multiple binning procedure allows us to establish that for a given N_{part} , events in central collisions are more densely packed than relatively peripheral collisions. Therefore, the properties of events with different initial N_{part} densities could be studied using multiple binning procedure.

Figure 2(b) shows $N_{\text{coll}}/N_{\text{part}}$ as a function of N_{part} . $N_{\text{coll}}/N_{\text{part}}$ represents number of binary collisions per participating nucleon. For a denser overlap area, a single N_{part} is expected to encounter larger number of binary collisions, hence should have larger N_{coll} . This is clearly observed in Fig. 2(b). For a given N_{part} , more central events in L+R binning have a larger number of binary collision per N_{part} . Such rare events with same N_{part} but very different interaction rate inside the collision region could help disentangle effect of initial state on measured final state observables. Such a selection of events could not be otherwise accessed using the standard centrality binning alone.

Figure 2(c) shows $dN_{\text{ch}}/d\eta$ as a function of N_{part} . The $dN_{\text{ch}}/d\eta$ is expected to increase with N_{part} . A larger number of binary collision per participant nucleon would lead to a larger value of $dN_{\text{ch}}/d\eta$ according to a simple two-component model of particle production [33]. In any given centrality, we observed a wide range of nucleon densities in L+R binning from Fig. 2(a) and Fig. 2(b). Therefore, a larger $dN_{\text{ch}}/d\eta$ is obtained for events in L+R bins belonging to more central collisions even for a fixed N_{part} . In other words, for a given N_{part} , it is possible to choose events with larger event activity using L+R binning. It is important to note that $dN_{\text{ch}}/d\eta$ is more correlated to N_{part} rather than N_{coll} in a collision event [34].¹

Figure 3(a,b) show ε_2 and v_2 calculated using event plane method as a function of $dN_{\text{ch}}/d\eta$. ε_2 is geometry driven and v_2 is shown to be proportional to ε_2 following $v_2 = \kappa\varepsilon_2$, where κ is the proportionality constant dependent particularly on equation of state and medium viscosity [35]. Because v_2 arises as a hydrodynamic response to ε_2 , the overall trend as a function of $dN_{\text{ch}}/d\eta$ are expected to be similar. As ε_2 increases from central to peripheral

¹ Further details on nature of $dN_{\text{ch}}/d\eta/N_{\text{part}}$ and $dN_{\text{ch}}/d\eta/N_{\text{coll}}$ as a function of N_{part} for different centralities are shown in Appendix A. The plots show that the difference in centrality and L+R binning for $dN_{\text{ch}}/d\eta$ mostly arises from N_{part} .

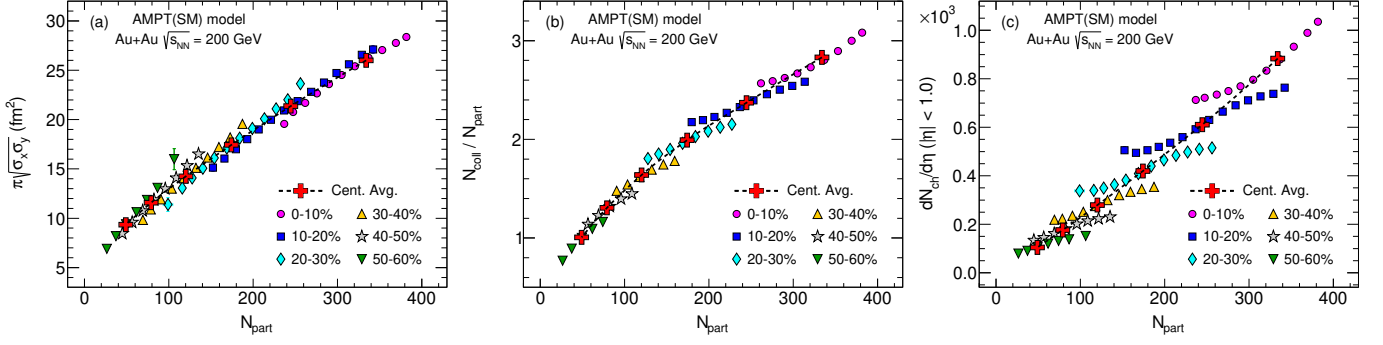


Fig. 2. (Color online) plots for minimum bias Au+Au collisions at $\sqrt{s_{NN}} = 200$ GeV. (Left) Overlap area vs N_{part} , (Middle) N_{coll}/N_{part} vs N_{part} , (Right) $dN_{ch}/d\eta$ vs N_{part} . Centrality average values are shown by ‘+’ marker in red color whereas the values for L+R binning in each centrality are shown in solid circles of different colors.

collisions, the magnitude of v_2 also increases. ε_2 in L+R binning shows a strong deviation and decreases sharper than the centrality averaged trend. From Fig. 2(a,b), it can be observed that for a given N_{part} , a more central event is more dense in L+R binning. This would lead to a more compact collision region which results in smaller ε_2 as clearly observed in Fig. 3(a). A similar behavior is observed for v_2 as shown in Fig. 3(b) as expected from the linear dependence of v_2 on ε_2 . In addition, L+R binning can be used to choose events with similar $dN_{ch}/d\eta$ but different v_2 . This could be particularly helpful in disentangling the effect of initial geometry and initial state interactions on the observed final state v_2 . For instance, using L+R binning within a given centrality, we could choose events with smaller area but larger eccentricity (or vice-versa) for a given N_{part} and then study how final state v_2 depends on these initial state parameters. Figure 3(b) also shows, L+R binning can be used to select events with same $dN_{ch}/d\eta$ but a higher v_2 for more central events. This, in turn, implies that certain anomalous events with higher eccentricity can arise from a more central collision. Having same v_2 across events with very different N_{ch} also provides an important handle to separate contribution from initial state geometry and fluctuations towards final state v_2 . L+R binning could especially help in studying the contribution from geometrical effects like deformation in nuclear shape, the dependence of which is different from factors such as system size, which contributes to fluctuations in final state v_2 .

On the other hand, ε_3 is known to be mostly fluctuation driven [36]. The ε_3 decreases from peripheral to central events owing to decreasing fluctuations [15] as observed in Fig. 3(c). The points corresponding to L+R binning for ε_3 vs. $dN_{ch}/d\eta$ is closer to the centrality averaged values than those for ε_2 . This approximately implies a one-to-one correspondence of v_3 with b unlike v_2 , as can be observed in Fig. 3(d). This could also suggest that the initial state fluctuations contributing to final state v_3 is mostly driven by fluctuations in b .

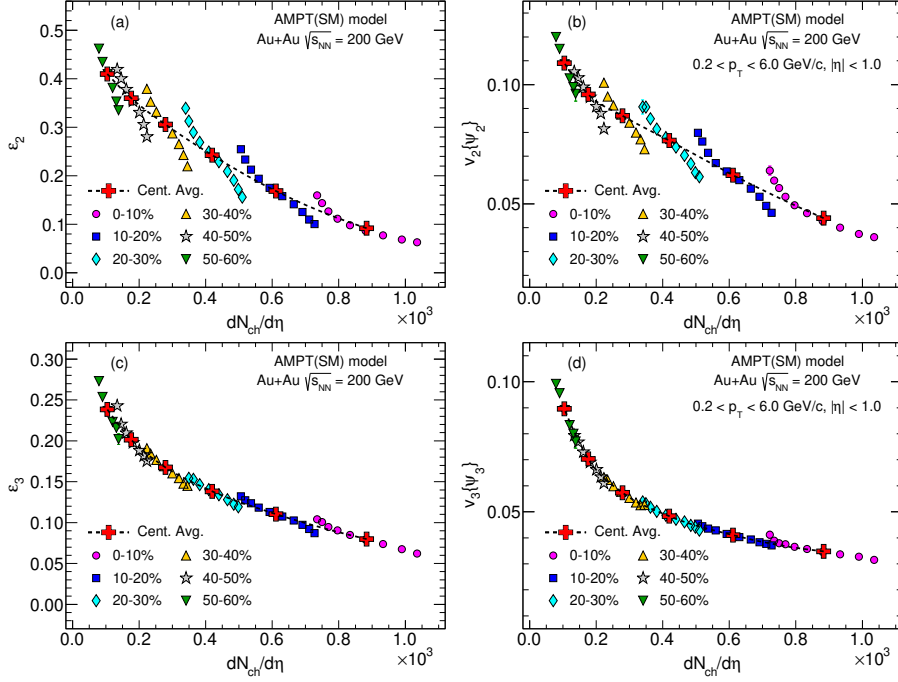


Fig. 3. (Color online) plots for minimum bias Au+Au collisions at $\sqrt{s_{NN}} = 200$ GeV. Top Row: (Left) ε_2 vs $dN_{ch}/d\eta$, (Right) v_2 vs $dN_{ch}/d\eta$; Bottom Row: (Left) ε_3 vs $dN_{ch}/d\eta$, (Right) v_3 vs $dN_{ch}/d\eta$. Centrality average values are shown by ‘+’ marker in red color whereas the values for L+R binning in each centrality are shown in solid circles of different colors.

The novelty of this work lies in quantification of difference in correlation between observables in centrality and L+R binning to improve access to initial state configurations. We assume a linear dependence in both the binning and extract the slopes using a linear fit. The fitting is performed separately for centrality averaged values and L+R binned values in each centrality. For centrality averaged values, we have fitted using one point on either side for a given centrality class. The range of fitting in L+R binning is varied over 2, 3 and 4 L+R bins on either side of the mean value for each centrality. The convergence of the slopes thus obtained for L+R binning is chosen as the nominal value to infer properties of rare events. We have also checked the value for the slope parameter taking the first coefficient from a 2nd order polynomial fit. The slope thus obtained was observed to be consistent with those obtained from linear fit. The centrality averaged slope reflects the correlation over a range of centralities whereas the slope for L+R bins reflects the correlation within a particular centrality. So, a relative difference between these two slopes for any given centrality shows the residual correlation on top of the centrality averaged trend and encodes additional details about the events that are otherwise hidden in standard centrality binning method. We define a quantity R_c which is the relative ratio between centrality averaged slope (S_c) and slope for the L+R binning (S_{ns}) for each centrality, $R_c = (S_{ns}/S_c) - 1$. If the final state observable is purely fluctuation driven such as impact parameter fluctuations or

uncertainties in nucleon positions, the R_c is expected to have a value of 0. The deviation from baseline of 0 denotes the extent by which a certain observable is dominated by dynamic effects other than impact parameter fluctuations or the uncertainties in nucleon positions.

The procedure to extract the slopes using linear fit is shown in Fig. 4(a) for $dN_{\text{ch}}/d\eta$ vs N_{part} . Figure 4(b) shows the extracted slopes and R_c as a function of centrality. The extracted slopes for centrality binning are shown in red dotted lines and those for L+R binning are shown in blue stars. From central to peripheral events, the slope decreases much faster in L+R binning than the slopes from centrality binning. This difference in slopes is directly reflected in the magnitude of R_c as shown in the bottom panel of Fig. 4(b). The slopes extracted from the two methods are observed to be closest for the most central events (0-10%). This is expected because of very similar magnitudes of $\rho(n_{\text{spec}}, N_{\text{part}})$ and $\rho(n_{\text{spec}}, N_{\text{ch}})$ as shown in Fig. 1(c). Therefore, one can obtain very little additional information on the correlation between $dN_{\text{ch}}/d\eta$ and N_{part} in L+R binning in comparison to centrality binning. From Fig. 4(a), one can observe an almost linear dependence of $dN_{\text{ch}}/d\eta$ with N_{part} in centrality binning using AMPT model for Au+Au collisions at $\sqrt{s_{\text{NN}}} = 200$ GeV. R_c is observed to increase from central to peripheral collisions. A deviation of R_c from baseline of 0 can be interpreted as a deviation from linearity of $dN_{\text{ch}}/d\eta$ in the final state to N_{part} from the initial state. Therefore, towards more peripheral centralities, the particle production in L+R binning can capture contributions from factors other than those contributing to particle production in just centrality binning. As we go from central to peripheral collisions, the particle production mechanism becomes more complicated than just a linear response to initial N_{part} . The multiple binning procedure can help in deciphering more details about the initial state configuration and energy deposition mechanism to understand the evolution of particle production.

Figure 5(a) shows slopes for b vs N_{part} in centrality and L+R binning. The slopes for centrality averaged values and L+R binned values are very close for all centralities. This observation can be also seen in Fig. 1(c) where for a given N_{part} , L+R binning and centrality binning correspond to the same b . In other words, because b has one to one correspondence to n_{spec} , the event selection between centrality and L+R binning is not biased.

Figure 5(b) shows slopes for S vs N_{part} in centrality and L+R binning. The slopes are positive because increasing N_{part} leads to a larger S . The R_c for S vs N_{part} is observed to decrease from central to peripheral collisions. A steady decrease in R_c implies a consistently increasing slope for L+R binning compared to centrality binning. This increasing difference in slopes implies a better access to events with larger S with similar N_{part} for more peripheral events. Therefore, using L+R binning it is possible to access events with larger S or smaller density at same N_{part} for 10–60% centrality. This could be leveraged to select on events with very different initial state densities at same N_{part} which could shed light on particle production mechanism and contribution of rare initial states to final state observables.

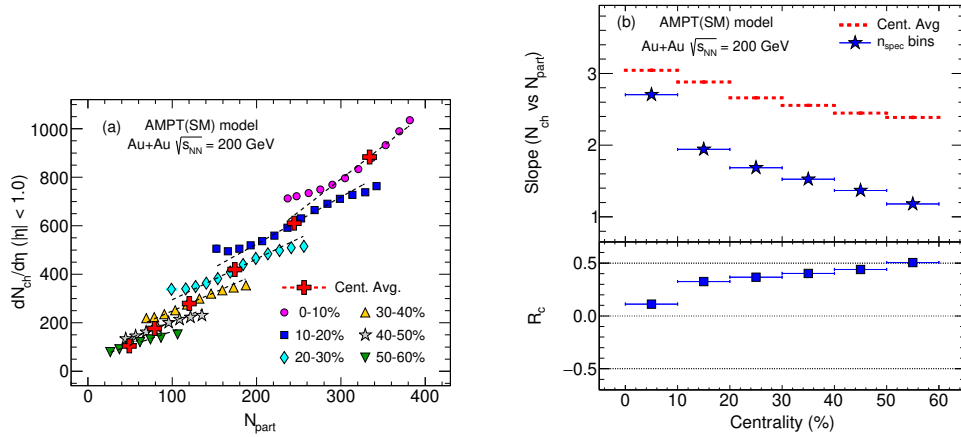


Fig. 4. (Color online) plots showing the method used to quantify the deviation of n_{spec} binned values from centrality trend in Au+Au collisions at $\sqrt{s_{\text{NN}}} = 200$ GeV. (Left) $dN_{\text{ch}}/d\eta$ vs N_{part} showing the linear fits for centrality averaged values and L+R bins for each centrality in dotted lines. (Right) The extracted slope shown as a function of centrality, red dotted line showing slope of the centrality averaged values and solid stars showing the average slope of the values in n_{spec} bin for each centrality, bottom panel shows the relative difference between slopes (R_c).

Figure 5(c) shows slopes for $N_{\text{coll}}/N_{\text{part}}$ vs N_{part} in centrality and L+R binning. The slopes are positive implying a increase in rate of binary collisions with increasing N_{part} . The slope in L+R binning is consistently smaller than the centrality averaged slope and R_c shows a maxima about mid-centrality. This shows that the rate of binary collision within each centrality have contributions other than just the N_{part} . One obvious source could be the S , which itself takes a range of values within each centrality and could lead to a larger $N_{\text{coll}}/N_{\text{part}}$ for smaller S and vice-versa (as also shown previously in Fig. 2(a)). The large magnitude of R_c also implies that L+R binning gives improved access to the events in which rate of interaction is lower for more peripheral events for a fixed N_{part} . In other words, it enables us to study events belonging to the same centrality, but with different rate of interactions which could result in different $dN_{\text{ch}}/d\eta$ in the final state (also shown in Fig. 2(c)). Thus, L+R binning can be used to shed light on how initial rate of interaction ($N_{\text{coll}}/N_{\text{part}}$) in different centralities impacts final state particle production mechanism.

Figure 5(d,e) shows slopes for v_2 and v_3 vs N_{part} and their respective R_c . v_2 being dominated by effects from the shape of initial geometry shows a larger R_c going from central to peripheral events. If the final state v_2 was purely driven by initial state fluctuations in participant positions, the slope of v_2 vs N_{part} would have been expected to be the same in centrality and L+R binning. This in turn would have lead to a R_c value of 0. The deviation from baseline of 0 denotes the extent by which v_2 is dominated by initial state geometry on top of the initial state fluctuations. Another interesting point to note is that in most central collisions, as the origin of v_2 is dominated by initial state

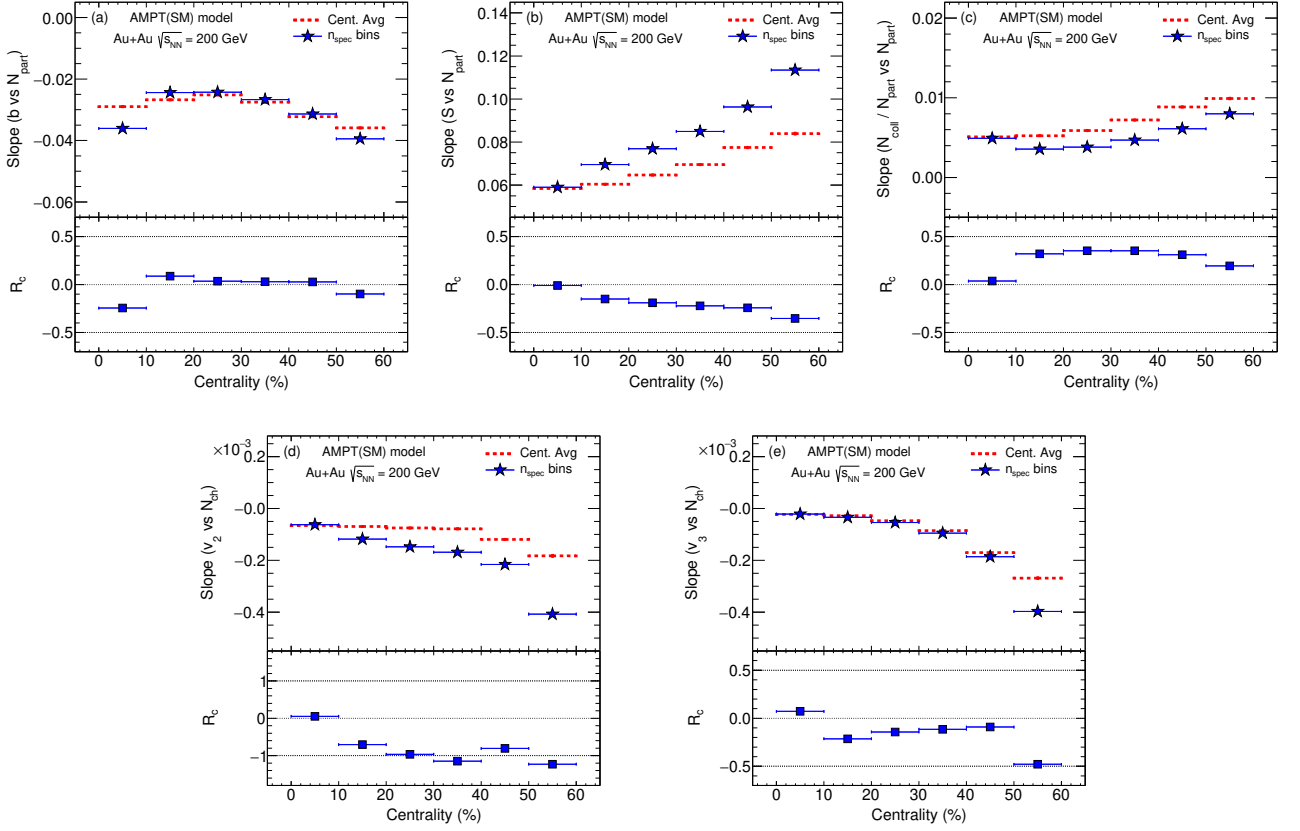


Fig. 5. (Color online) Slope for centrality averaged values (red dashed line) and for L+R bins (solid stars) extracted using local linear fits. Top Row:(Left) Slopes for b vs N_{part} , (Middle) Slopes for S vs N_{part} , (Right) Slopes for $N_{\text{coll}}/N_{\text{part}}$ vs N_{part} . Bottom Row: (Left) Slopes for v_2 vs N_{ch} , (Right) Slopes for v_3 vs N_{ch} . Bottom panel in all figures show relative ratio between slopes, R_c as a function of Centrality.

fluctuations [37], the R_c parameter is close to 0 for 0–10% centrality. For v_3 , the slopes from centrality and L+R binning for are very close over a wide range in centrality (0–50%). This reinforces the argument that v_3 arises mostly from initial state fluctuations and the additional information that could be obtained from L+R binning in this case is quite limited.

4 Conclusion

We showed that n_{spec} could be used as an additional classifier of event characteristics on top of N_{ch} owing to very small correlation between n_{spec} and N_{ch} . A new method was developed to quantify the difference in slope of correlations between observables in centrality and L+R binning using R_c . A large magnitude of R_c , upto 50% was observed for the correlation between S and N_{part} . This enables us to choose very different initial overlap area for the same N_{part} . Such

a selection over a wide range of overlap area at fixed N_{part} via L+R binning also leads to widely varying initial state densities, by about 40%. The resulting variation in initial state densities and interaction rates also leads to a wide range of $dN_{\text{ch}}/d\eta$ for a given N_{part} . The increasing magnitude of R_c for $dN_{\text{ch}}/d\eta$ vs N_{part} towards peripheral centrality might point towards the non-linear contributions in initial state configurations or in energy deposition mechanism on top of the linear contribution from N_{part} in a simple two-component model. The behavior of observables which are known to have dynamical contributions from initial state on top of impact parameter fluctuations are observed to be very different between centrality averaged and L+R binned values. As a result, we observe a large magnitude of R_c for correlation between v_2 and N_{ch} whereas, the R_c for v_3 vs N_{ch} is very small, $\sim 10\%$ on an average. Therefore, a separation of the contribution of initial state geometry from those arising purely from fluctuations could be obtained for v_2 using R_c .

L+R binning provides a unique handle to differentiate between events with widely different initial state density and rate of binary collisions even at a fixed N_{part} . The effect of such rare and widely varying initial state configurations within each centrality class could not be accessed by a standard centrality binning. In addition, because of the reduced sensitivity of R_c towards initial state fluctuations, it could also potentially aide in separating the contributions of geometry and initial state fluctuations towards final state v_2 . Such discriminating power of L+R binning procedure could be leveraged in future to select on events with rare properties to disentangle the impact of several initial state parameters on final state observables. In particular, this novel binning procedure could be applied to probe properties of initial states in heavy-ion collision systems. Data from ZDC detector systems installed at RHIC and LHC could be specifically used to get event-by-event spectator neutrons for a more realistic test of this method. Further improvement in ZDC design in future experiments could help increase the single neutron peak resolution. Such improvements would also allow us to extend the centrality range in which the multiple binning procedure could be implemented. It would be of great interest to study the implication of L+R binning for smaller or deformed systems which are known to have additional contribution to final state fluctuation measure when compared to larger, spherical systems.

References

1. D. Teaney, E. Shuryak, *Phys. Rev. Lett.* **86**, (2001) 4783-4786.
2. J. Adams et. al (STAR Collaboration), *Nucl. Phys. A* **757**, (2005) 102.
3. J. Bernhard et. al, *Phys. Rev. C* **94**, (2016) 024907.
4. D. Everett et. al (JETSCAPE Collaboration), *Phys. Rev. C* **103**, (2021) 054904.
5. G. Nijs et. al, *Phys. Rev. Lett.* **126**, (2021) 202301.

6. H. J Drescher et. al, *Phys. Rev. C* **76**, (2007) 024905.
7. P. Romatschke and U. Romatschke, *Phys. Rev. Lett.* **99**, (2007) 172301.
8. M. Luzum and P. Romatschke, *Phys. Rev. C* **78**, (2008) 034915 [Erratum: *Phys. Rev. C* **79**, (2009) 039903].
9. V. Roy et. al, *Phys. Rev. C* **86**, (2012) 014902.
10. H. Song et. al, *Phys. Rev. Lett.* **106**, (2011) 192301 [Erratum: *Phys. Rev. Lett.* **109**, (2012) 139904].
11. V. Roy et. al, *J. Phys. G* **40**, (2013) 065103.
12. M. L Miller et. al, *Ann. Rev. Nucl. Part. Sci.* **57**, (2007) 205-243.
13. C. Loizides, *Phys. Rev. C* **94**, (2016) 024914.
14. A. M Poskanzer and S. A Voloshin, *Phys. Rev. C* **58**, (1998) 1671.
15. B. Alver and G. Roland, *Phys. Rev. C* **81**, (2010) 054905 [Erratum: *Phys. Rev. C* **82**, (2010) 039903].
16. C. Gale et. al, *Int. J. Mod. Phys. A* **28**, (2013) 1340011.
17. U. Heinz and R. Snellings, *Ann. Rev. Nucl. Part. Sci.* **63**, (2013) 123.
18. F. G Gardim et. al, *Phys. Rev. C* **85**, (2012) 024908.
19. J. Xu, C. M Ko, *Phys. Rev. C* **84**, (2011) 044907.
20. J. Xu, C. M Ko, *Phys. Rev. C* **84**, (2011) 014903.
21. V. Bairathi et. al, *Phys. Rev. C* **91**, (2015) 054903.
22. S. Sombun et. al, *J. Phys. G* **45**, (2018) 025101.
23. V. Bairathi et. al, *Phys. Lett. B* **754**, (2016) 144-150.
24. Yi-Fei Xu et. al, *Nucl. Sci. Tech.* **27**, (2016) 126.
25. E. G Judd et. al, *Nucl. Instrum. Meth. A* **902**, (2018) 228.
26. Z. W Lin et. al, *Phys. Rev. C* **72**, (2005) 064901.
27. X.-N. Wang and M. Gyulassy, *Phys. Rev. D* **44**, (1991) 3501-3516.
28. B. Zhang, *Comput. Phys. Commun.* **109**, (1998) 193.
29. B. Andersson et. al, *Z. Phys. C* **20**, (1983) 317.
30. J. Adam et. al (ALICE Collaboration), *JHEP* **2015**, (2015) 97.
31. ATLAS Collaboration, arXiv:2205.00039 [nucl-ex].
32. C. Loizides et. al, *SoftwareX* **1-2**, (2015) 13-18.
33. D. Kharzeev and M. Nardi, *Phys. Lett. B* **507**, (2001) 121.
34. J. S Moreland et. al, *Phys. Rev. C* **92**, (2015) 011901.
35. R. S. Bhalerao et. al, *Phys. Rev. C* **84**, (2011) 034910.
36. G. Kh. Eyyubova et. al, *J. Phys. G* **48**, (2021) 095101.
37. H. Petersen et. al, *Phys. Rev. C* **82**, (2010) 041901.

A Appendix

Additional plots to study origin of $dN_{\text{ch}}/d\eta$ from N_{coll} and N_{part} are given below.

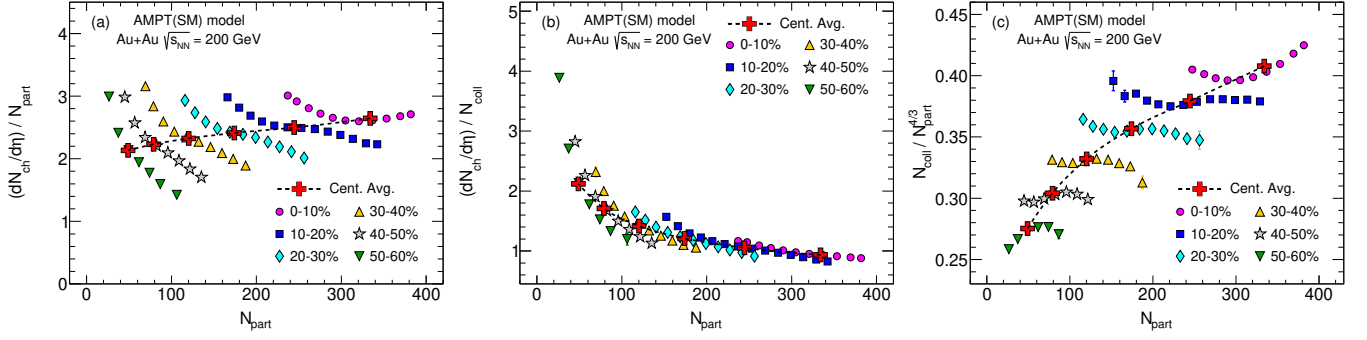


Fig. 6. (Color online) plots for minimum bias Au+Au collisions at $\sqrt{s_{\text{NN}}} = 200$ GeV. (Left) $dN_{\text{ch}}/d\eta/N_{\text{part}}$ vs N_{part} ; (Center) $dN_{\text{ch}}/d\eta/N_{\text{coll}}$ vs N_{part} ; (Right) Geometrical scaling $N_{\text{coll}}/(N_{\text{part}})^{4/3}$ vs N_{part} [12]. Centrality average values are shown by ‘+’ marker in red color whereas the values for L+R binning in each centrality are shown in solid circles of different colors.